NASA TECHNICAL MEMORANDUM

NASA TM X- 68014

NASA TM X- 68014

EXPERIMENTS ON THE STABILITY OF VARIOUS WATER-LUBRICATED FIXED GEOMETRY HYDRODYNAMIC JOURNAL BEARINGS AT ZERO LOAD

by Fredrick T. Schuller
Lewis Research Center
Cleveland, Ohio

TECHNICAL PAPER proposed for presentation at
Lubrication Conference sponsored by the American
Society of Mechanical Engineers and the American
Society of Lubrication Engineers
New York, New York, October 9-12, 1972

ABSTRACT

Hydrodynamic journal bearing stability tests were conducted with 3.8 centimeter (1.5 in.) diameter, 3.8 centimeter (1.5 in.) long fixed geometry bearings in water at 300 K (80° F) with zero load. Five fixed goemetry bearings were rated in order of diminishing stability as follows: (1) three-tilted-lobe bearing (offset factor of 1.0), (2) herringbone-groove bearing, (3) one-segment, three-pod, shrouded Rayleigh-step bearing, (4) three-tilted-lobe journal with axial grooves (offset factor of 1.0) mated with a plain bearing, and (5) three-centrally-lobed bearing with axial grooves (offset factor of 0.5). The various parameters that affect the stability of each bearing configuration were investigated.

E-6710

EXPERIMENTS ON THE STABILITY OF VARIOUS WATER-LUBRICATED FIXED GEOMETRY HYDRODYNAMIC JOURNAL BEARINGS AT ZERO LOAD

by Fredrick T. Schuller

Lewis Research Center
National Aeronautics and Space Administration
Cleveland, Ohio

E-6710

SUMMARY

Stability tests were conducted with 3.8 centimeter- (1.5 in.-) diameter, 3.8 centimeter- (1.5 in.-) long, fixed geometry hydrodynamic journal bearings in water at 300 K (80° F) with zero load. Five fixed geometry bearings were rated in order of diminishing stability as follows: (1) three-tilted-lobe bearing (offset factor of 1.0), (2) herringbone-groove bearing, (3) one-segment, three-pad, shrouded Rayleigh-step bearing, (4) three-tilted-lobe journal with axial grooves (offset factor of 1.0) mated with a plain bearing, and (5) three-centrally-lobed bearing with axial grooves (offset factor of 0.5).

Maximum stability in lobed bearings and journals is achieved when the lobes are tilted so that the points of minimum film thickness occur near the trailing edges. The herringbone-groove journals had a maximum stability (maximum fractional frequency whirl onset speed) when the groove to ridge clearance ratio was closest to 2.1, as predicted by incompressible flow theory. The one-segment, three-pad shrouded Rayleigh-step bearing configuration was the most stable of the four step-bearing configurations tested. The tilted-lobe journals mated with plain bearings were unique in that, in some tests, the bearings could be run to a shaft speed twice the shaft speed at which initial fractional frequency whirl occurred before any sign of bearing distress was observed.

INTRODUCTION

The ability of a journal bearing to inhibit self-excited fractional frequency whirl is of prime importance for successful operation of rotating machinery at conditions of high speed and low loads with a low-viscosity fluid, such as water, as the lubricant. In this type of whirl, the journal center orbits the bearing center at an angular velocity about one-half that of the journal around its own center. Such whirling can fail a bearing, if the amplitude of whirl grows and is not limited. It is desirable, therefore, to select a bearing geometry that has a high degree of stability.

Tilting-pad bearings are exceptionally stable but are complex since they are composed of several parts and may be subject to pivot surface damage (ref. 1). Fixed geometry bearings do not have the disadvantage of

complexity, but they are not as stable as the tilting-pad bearing. It is known that discontinuous films, such as those produced by steps and grooves, tend to stabilize a bearing (ref. 2). One such bearing that showed good stability properties is the herringbone-groove bearing (refs. 3 and 4). The Rayleigh-step bearing is another configuration that is worthy of stability investigation. Another fixed geometry bearing that has shown promise is the lobed bearing (refs. 5 and 6), which has a marked similarity to the tilting-pad bearing except that its pads (lobes) are fixed in one position.

Most of the research on lobed bearing stability has been done with bearings that are centrally-lobed, which results in converging-diverging films. In a centrally-lobed bearing, only the converging wedge portion of the arc of each lobe is active in generating load capacity. If the lobe is tilted toward the shaft at the trailing edge of the lobe, the minimum film thickness occurs nearer the trailing edge of the lobe, and a pressure profile is built up over a larger portion of the lobe arc, which increases its load capacity (ref. 7). Reference 7 reports an improvement in the stability of a tilted-lobe bearing over those that were centrally lobed.

In the above investigations on lobed bearings, the nonrotating member (the bearing) had the lobed contour and was run with a plain rotating journal. Reference 6 reports an analytical investigation of a centrally-lobed rotor with three or more lobes running stably in a plain bearing. Some experimental results for a three-centrally-lobed rotor are also included, which verify the theoretical analysis.

In the investigation reported herein various fixed geometry bearings were studied to determine the important parameters that affect their stability. A comparison of the stability of each of the bearings is also given.

A general description of the fixed geometry bearings tested is given as follows: (1) herringbone-groove bearings, (2) Rayleigh-step bearings, (3) three-lobed bearings, and (4) three-lobed journals mated with a plain bearing.

The test bearings had a nominal 3.8 centimeter (1.5 in.) diameter and were 3.8 centimeter (1.5 in.) long. They were submerged in water at an average temperature of 300 K (80° F) and were operated hydrodynamically with zero load. This work was initially reported in references 8 to 13.

SYMBOLS

a preload (ellipticity), mm; in.

C bearing radial clearance, mm; in.

C_S radial clearance in step region when bearing and journal are concentric, C + S, mm; in.

C_0 bearing radial clearance at zero preload, $R_P - R$, mm; in.

D journal diameter, cm; in.

g gravitational constant, m/sec^2; $in./sec^2$

H herringbone groove clearance to ridge clearance ratio, h_g/C

H_L film thickness ratio, (h_g/C), for herringbone groove bearings

h_g groove clearance, C + S, mm; in.

k film thickness ratio $(1 + \Delta R_L/C)$, for lobed bearings

k_r film thickness ratio (C_S/C), for Rayleigh-step bearings

L bearing length, cm; in.

M rotor mass per bearing, W_r/g, kg; $(lb)(sec^2)/in.$

$\bar{M}$ dimensionless mass parameter, $MP_aC^5/2\mu^2LR^5$

$\bar{M}_0$ dimensionless rotor mass parameter, $C_0MN_S/\mu DL(R/C_0)^2$ (ref. 5)

N_S journal speed, rps

N_W journal fractional frequency whirl onset speed at zero load, rpm

P_a atmospheric pressure, N/m^2 abs; psia

R journal radius, cm; in.

R_B bearing radius, cm; in.

ΔR_L leading edge entrance wedge thickness, mm; in.

R_P lobe radius, cm; in.

R_{PC} radius of pitch circle, cm; in.

S depth of herringbone groove or Rayleigh step, mm; in.

W_r total weight of test vessel, N; lb

α offset factor, θ/β

β sector arc length, deg

Γ dimensionless speed parameter, $6\mu\omega R^2/P_a C^2$

γ angle subtended by ridge (Rayleigh-step bearing), deg

δ preload coefficient, $a/(R_p - R)$

ζ angle subtended by lubrication groove, (Rayleigh-step bearing), deg

θ arc length from leading edge of sector to the line along which the lobe is preloaded radially, deg

μ lubricant dynamic viscosity, (N)(sec)/m^2; (lb)(sec)/$in.^2$

ϕ angle subtended by step (Rayleigh-step bearing), deg

ψ ratio of ridge angle to total angle of ridge-step-groove combination (ridge to pad arc ratio, Rayleigh-step bearing) $\gamma/(\gamma + \phi + \zeta)$

ω journal angular speed, rad/sec

TEST BEARINGS

Herringbone-Groove Bearings

Herringbone-groove journal bearings of six configurations, three journals having 10, 20, and 40 full grooves and three having 10, 20, and 40 partial grooves (fig. 1), were evaluated. Grooving extended beyond the bearing sleeves at each end to ensure an adequate lubricant supply. The partially grooved journals had a circumferential land centrally located along the length of the bearing. The width of the circumferential land was one-third the bearing length (fig. 1(b)). The fully grooved journals had herringbone grooves that met midway along the bearing axial length. To reduce the number of new journals required, the outside diameter of the journals with large groove depths was ground after testing to reduce the groove depth, and the journal was reused.

The herringbone groove apex angle was set at 33° and the groove to ridge width ratio at 1.0. These values yield a maximum radial force at a compressibility number of zero for a compressible lubricant (ref. 4). This approximates the conditions existing with an incompressible lubricant.

Rayleigh-Step Bearings

In the description of the Rayleigh-step bearing a definition of bearing terms is necessary as follows:

Configuration - relative disposition of pads and segments (figs. 2(a) to (c))

Feed groove - axial groove that runs the length of the segment and feeds lubricant to the bearing (fig. 2(c))

Geometry - arc lengths and step depths that describe the step and ridge regions (fig. 3)

Pad - a combination of feed groove and step and ridge regions (fig. 2(c))

Ridge region - raised area of a pad not including the shrouds (fig. 2)

Segment - an independently acting 360° region; it may incorporate one or more pads (fig. 2(b))

Shroud - side rails at the axial ends of the segment in the step region that act as a dam (fig. 2)

Step region - relieved area of a pad (fig. 2)

Rayleigh-step bearings of four different configurations were evaluated (fig. 2). One consisted of one segment running the length of the bearing with one pad in its circumference as shown in figure 2(a). Another consisted of three circumferential segments of equal length, side by side, separated from each other by grooves as shown in figure 2(b). Each segment contained one pad that was displaced 120° circumferentially with respect to the others to achieve symmetry in the bearing. The length of each segment was one-third the total length of the bearing. One set of such bearings had a ridge to pad arc ratio ψ (fig. 3) of 0.40 and another set of bearings had a ψ of 0.49. These ridge to pad arc ratios were selected on the basis of the load capacity results of reference 14. Since the load capacity curve of reference 14 has a rather flat peak, both arc ratios represent conditions which yield maximum load capacity for a single-sector Rayleigh-step bearing at the small eccentricity ratios (ε = 0 to 0.3), that can be expected with a bearing under zero load.

The third Rayleigh-step bearing configuration that was evaluated is shown in figure 2(c). It consisted of three pads extending the entire length of the bearing. One set of such bearings had a ridge to pad arc ratio ψ of 0.27 and another set had a ψ of 0.45. The ratios chosen were based on analytical work on load capacity for three-pad Rayleigh-step bearings at an eccentricity ratio of 0.1 reported in reference 15.

One of the one-segment, three-pad bearings with shrouds and a ridge to pad arc ratio ψ of 0.45 had its shrouds machined off after test. It was then rerun without shrouds. This was the fourth configuration tested.

The width of the shroud for the three-segment, single-pad bearing was 1.5 millimeters (0.06 in.) and 4.8 millimeters (0.19 in.) for the one-segment, three-pad, and one-segment, one-pad bearings. The bottom corners of the steps in the bearings were not sharp but had a machined radius of approximately 0.97 centimeter (0.38 in.).

Figure 3 shows the parameters that define the Rayleigh-step bearing geometry. The angle γ is defined as the angle subtended by the ridge region; ϕ, the angle subtended by the step region; and ζ, the angle subtended by the lubrication groove. The latter angle ζ is included since it was used in the analysis of references 14 and 15. Although this angle is normally small and may not be important for the one- and three-step configuration employed in this investigation, it can become important in an analysis of a Rayleigh-step bearing with a large number of pads. The symbol C in figure 3 is the radial clearance between the journal and the ridge region and C_S is the radial clearance in the step region when the journal is in a concentric position in the bearing. The depth of the step S is then $C_S - C$.

Three-Lobed Bearings

Three-centrally-lobed bearings with and without axial grooves were evaluated. The bearings were lobed by the use of shims as shown in figure 4(a). The height of the lobes, ΔR_L (fig. 4(b)), was determined from circumferential profile traces of the inside surface of the shimmed test bearings.

Three sector-bearings consisting of three 115^o tilted lobes, mounted in a solid housing by hold-down screws (figs. 5(a) and (b)), were evaluated. Each sector of one particular bearing assembly was ground to its specified contour while it was the only sector assembled in the housing. Three sectors with identical contours were then assembled in a common housing to form a three-tilted-lobe bearing, as shown in figure 5(a).

Two different contours were employed in the bearing sectors to give one bearing a converging-diverging film (fig. 5(c)) in operation and another bearing a wholly converging film (fig. 5(d)).

Figure 4(b) shows the parameters which define the centrally-lobed bearing geometry. The angle θ is defined as the arc length from the leading edge of a sector to the point of minimum film thickness at zero eccentricity. In this case $\theta = 0.5\ \beta$. The offset factor $\alpha = \theta/\beta$ for the centrally-lobed bearing is, therefore, 0.5. Figures 5(c) and (d) show the parameters which define the tilted-lobe bearing geometries with offset factors of 0.6 and 1.0, respectively. Circumferential profile traces were made of the internal surface of each bearing configuration in three planes along the length of the bearing to obtain the leading edge entrance wedge thickness ΔR_L (figs. 4(b), 5(c) and (d)).

Three-Lobe Journals Mated with Plain Bearings

Basically, two different contours were employed in the journals to give one a wholly converging film profile in operation (fig. 6(a), offset factor of 1.0) and another a converging-diverging film (fig. 6(b), offset factor of 0.5). A third configuration was obtained by machining three

axial grooves in the journal with the wholly converging film (fig. 6(c)). In the case of the tilted-lobe journal, $\theta = \beta$, figure 6(a). The offset factor $\alpha = \theta/\beta$ is therefore 1.0. The offset factor for the centrally-lobed journal is $\theta/\beta = 60^{\circ}/120^{\circ}$ or 0.5 (fig. 6(b)).

Bearing Test Apparatus

The test apparatus and its associated parts are shown in figure 7. The shaft is positioned vertically so that gravity forces do not load the bearing. The test vessel, which also serves as the test bearing housing, floats between the upper and lower gas bearings. Bearing torque can be measured, if desired, by a force transducer attached to the floating test vessel. The test shaft was mounted on two support ball bearings that were preloaded to about 890 newtons (200 lb) by a wave spring. This preload was necessary to ensure a minimum amount of shaft runout.

Movement of the test vessel during a test is measured by orthogonally mounted capacitance probes outside the test vessel. The output of the probes is connected to an x-y display on an oscilloscope where the test vessel motion can be observed. The orbital frequency of the test vessel motion was measured by a frequency counter.

Test Procedure

Test shaft speed was increased in increments ranging from 100 rpm in some tests to 1000 rpm in others. The bearings were run at zero load throughout the entire test. Onset of whirl was noted by observing the bearing housing motion on the oscilloscope screen (ref. 8). Shaft speed was recorded at this time. Damage to the test bearing and journal due to fractional-frequency whirl was prevented by reducing the speed immediately after photographing the whirl pattern on the oscilloscope screen.

Usually, in any bearing stability investigation, the motion of the test shaft is monitored. However, in the experiments reported herein, the motion of the bearing with its massive housing (total weight 50 kg, 110 lb) was monitored. In order to establish the validity of the stability data obtained in this investigation, a three-axial-groove bearing, under light radial loads, was run in water with a plain journal. The results were compared with the theoretical curve of a 100° partial-arc bearing (ref. 16) as shown in figure 8. (The 100° partial-arc bearing has stability characteristics similar to those of the three-axial-groove bearing.) Excellent correlation was obtained between theoretical and experimental data, which indicated that the test apparatus and its monitoring system were highly reliable.

RESULTS AND DISCUSSION

Herringbone Groove Bearings

Six journals having different groove geometries, as shown in figure 1, with a total of fifteen different groove depths were investigated. A total of 67 bearing stability tests was conducted at radial clearances ranging from 0.008 to 0.046 millimeter (300 to 1800 μin.), and groove depths ranging from 0.009 to 0.085 millimeter (340 to 3350 μin.).

Although there are individual differences in the stability characteristics of herringbone-grooved journals when considering the effect of number of grooves and groove length, these differences are seen to be minimal when all the data for bearings of approximately the same groove depths are grouped to form one stability plot. The theoretical stability analysis of a journal bearing in reference 8 showed that the important parameters to consider are the dimensionless mass parameter M and the dimensionless speed parameter Γ, as shown in figure 9. A smooth curve has been drawn through the collective stability data for all journal bearings having 40, 20, and 10 partial and full grooves ranging in depth from 0.032 to 0.043 millimeters (1280 to 1700 μin.). In the area labeled stable operation, to the left of the experimental curve, the bearings ran stably at zero load; to the right of the curve, fractional frequency whirl occurred.

The herringbone groove helix angle, 33°, and groove to ridge width ratio, 1, were set at those values which yield a maximum radial force as calculated from reference 4 at a compressibility number of zero for a compressible lubricant. This approximates the conditions existing with an incompressible lubricant. The optimum groove to ridge clearance ratio, H, is 2.1 for this condition (ref. 4). Figure 10 shows plots of H against zero load whirl onset speed, N_W, at four different clearance values. N_W at each clearance reached a maximum at an H value very close to 2.1, indicating that this value of H is optimum for both maximum radial force and stability. Once a value for radial clearance has been chosen for a particular herringbone-groove journal bearing, the groove depth for maximum stability can be reliably determined from the $H = 2.1$ value for incompressible fluids. A more complete analysis of the herringbone groove data is recorded in references 8 and 9.

Rayleigh Step Bearings

Eighty stability tests were conducted on Rayleigh-step journal bearings of the four different configurations discussed in the section Test Bearings. Each configuration was run at four different clearances at various step depths. The clearances ranged from 0.010 to 0.052 millimeters (400 to 2050 μin.), and the step depths ranged from 0.015 to 0.094 millimeters (600 to 3700 μin.).

The configurations tested ranked generally in the following order of

diminishing stability: one-segment, three-pad shrouded; one segment, one-pad shrouded; one-segment, three-pad unshrouded; and three-segment, one-pad shrouded.

The stability of a three-segment, one-pad shrouded and a one-segment, three-pad shrouded bearing was not appreciably affected by a change in ridge to pad arc ratio, ψ, from 0.40 to 0.49 and 0.27 to 0.45, respectively, as shown in figure 11(a) and (b).

The two curves in figure 12 show the threshold of stability of a shrouded and unshrouded one-segment, three-pad bearing with a ψ of 0.45. The data for both were obtained from the same bearing which was first run with shrouds. The shrouds were then machined off and the bearing was rerun without shrouds. Figure 12 shows that a substantial increase in stability can be gained by using shrouds since the dimensionless mass $\overline{M}$ for the shrouded bearing is always greater than that for the unshrouded bearing over the entire range of dimensionless speeds Γ tested.

Whirl onset speed, N_W, is plotted against radial clearance in figure 13(a) for five different values of step depth for the one-segment, three-pad shrouded bearings, in order to facilitate the design of optimum-geometry bearings. Because of the close similarity of the stability data between the bearings with a ψ of 0.27 and 0.45 (fig. 11(b)) the following design curves can be applied to either. Design curves for the three-segment, one-pad shrouded bearing were not considered here because of their relatively low stability. The one-segment, one-pad configuration was not considered because of its limitation of preferential loading direction and the fact that insufficient stability data were available. The values of film thickness ratio $k_r = C_S/C$ are given in figure 13(a) for each data point and represent the ratio of the clearance at the step region to the clearance at the ridge region of each bearing when the shaft is concentric in the bearing (see fig. 3). The four vertical dashed lines, drawn at arbitrary clearance values of 0.018, 0.025, 0.038, and 0.051 millimeters (700, 1000, 1500, and 2000 μin.), intersect the stability curves at various values of whirl onset speed. The curves in figure 13(b) were obtained by cross plotting the data in figure 13(a) at the four different values of clearance using whirl speed N_W and film thickness ratio k_r as variables. Straight line interpolation was used to obtain values of k_r for the cross plot. In figure 13(b) there is an optimum value of k_r at any given C and this optimum is a function of C. Figure 13(b) also shows that stability becomes more sensitive to k_r as C increases. It also shows that the optimum film thickness ratio k_r decreases from 2.8 to 1.6 as the clearance increases from 0.018 to 0.051 millimeters (700 to 2000 μin.). For eccentricity ratios less than 0.2, an optimal film thickness ratio of 1.7 was reported in reference 14, when using the criterion of load capacity. The optimal k_r value is therefore considerably higher (1.6 to 2.8) when using the criterion of stability as opposed to load capacity. For design purposes a k_r of 2 can be used; this will result in a bearing with close to optimum stability over a wide range of clearances.

A more detailed study of the Rayleigh-step bearing is contained in reference 10.

Three-Lobe Bearings

A total of 39 stability tests was performed on two types of centrally-lobed three-lobe bearings. One type had an axial groove separating each lobe arc and the other type had no grooves. Bearings of each type having a variety of lobe heights were run at a number of different radial clearances. The clearances varied from 0.009 to 0.052 millimeters (350 to 2050 μin.), and the lobe heights from 0 to 0.102 millimeter (0 to 4000 μin.).

Stable operation of a three-centrally-lobed bearing without axial grooves was impossible to attain at clearances above 0.018 millimeter (700 μin.) over a range of lobe heights from 0.025 to 0.102 millimeter (1000 to 4000 μin.).

The experimental results of three-centrally-lobed bearings with axial grooves are compared with theoretical curves for similar bearings in figure 14. The solid curves are from reference 5 and show the theoretical stability threshold of axially-grooved three-lobe bearings that are centrally lobed. Since the Reynolds number of the experimental points reported herein fell within the range of 0 to 2000, both curves have been included. The experimental data were plotted using the parameters of reference 5 and show fair agreement with the theoretical values for the centrally-lobed bearing (offset factor $\alpha = 0.5$). Theory predicts a larger range of stable operation than was observed experimentally.

Experimental results shown in figure 15 indicate that an optimum value of preload coefficient exists at any given clearance, and this optimum is a function of clearance. The preload coefficient, $\delta = a/(R_p - R)$, at the points of optimum locus, increases from about 0.54 to 0.78 as the clearance is reduced from 0.046 to 0.015 millimeter (1800 to 600 μin.).

In order to study the effect of offset factor (θ/β) on stability, sixteen tests were performed on bearings with offset factors of 0.6 and 1.0. Each offset factor was run at four different radial clearances at each of four different leading edge entrance wedge thickness ΔR_L, which varied from 0.013 to 0.107 millimeter (500 to 4200 μin.).

Figure 16 shows a comparison of the stability of three-lobe bearings with various offsets including the centrally-lobed bearing which has an offset factor of 0.5. Whirl speed is plotted against radial clearance for bearings of three different offset factors, 0.5, 0.6, 1.0. The data points for these three bearing types correspond to the points of maximum stability (optimum locus curve) obtained in a similar manner as those for the Rayleigh-step bearing shown in figures 13(a) and (b). As the offset factor is increased from 0.5 to 1.0 in figure 16, the curves shift to the upper right at a shallower slope, which indicates an increase in

stability and less sensitivity to clearance.

An analytical study of the three-lobe bearing was reported in reference 17, which showed that maximum stability for a three-lobe bearing with an $L/D = 1$ occurred at an offset factor of about 0.9. This agrees with the experimental data of figure 16, which shows an offset factor of 1.0 to be more stable than an offset factor of 0.5 or 0.6. References 11 and 12 contain a more detailed investigation of the centrally-lobed and tilted-lobe journal bearing, respectively.

Three-Lobe Journals Mated with Plain Bearings

Fifty stability tests were performed on the three types of lobed journal bearings described in the section TEST BEARINGS. The leading edge entrance wedge thickness varied from 0.010 to 0.178 millimeter (400 to 7000 μin.) and the radial clearances ranged from 0.015 to 0.048 millimeter (600 to 1900 μin.).

Figure 17 shows that the wholly-converging film configuration (tilted-lobe) is clearly more stable than the converging-diverging configuration (centrally-lobed), except at the higher clearance values, approximately 0.048 millimeter (1900 μin.) where their stabilities tend to be equal. Both curves were plotted from data obtained with identical leading edge entrance wedge thicknesses of 0.023 millimeter (900 μin.) and neither had axial grooves in the journal. Because of the relatively poor stability of the centrally-lobed journal compared with that of the tilted-lobe journal, further investigation of only the latter was undertaken.

Figures 18(a) and (b) show that there is an optimum value of k at any given C for both the ungrooved and grooved journals, and this optimum is strongly dependent on C. Stability for both journal types becomes more sensitive to k as C increases. The differences in stability characteristics of the ungrooved and grooved journal configuration are apparent when the magnitude and range of k for both are considered. Optimum k for the ungrooved journal decreased from 6.7 to 4.0 (fig. 18(a)) whereas for the grooved journal, k decreased from 1.92 to 1.55 (fig. 18(b)) as the clearance was increased from 0.018 to 0.046 millimeter (700 to 1800 μin.). The stability at optimum k for the grooved journal was generally greater than that for the ungrooved journal over the range of clearances tested. However, the stability curves of the ungrooved journal had much flatter peaks than those of the grooved journal which could make the former configuration more desirable for the designer because of its lesser sensitivity to changes in film thickness ratio, although some sacrifice in stability would result.

The reason for the upswing in the 0.018 and 0.023 millimeter (700 to 900 μin.) clearance curves for the ungrooved journal, figure 18(a), at k values of 2.3 and 2.1, respectively, is not completely clear. It is probably due to slight misalinement of the bearing with the journal.

This would tend to preload the bearing and give it some added stability under the tight clearance conditions, 0.018 and 0.023 millimeter (700 to 900 μin.), coupled with the small entrance wedge film thicknesses, ΔR_L, which are present at these small k values (see ref. 18). At higher clearances, above 0.023 millimeter (900 μin.) and/or higher ΔR_L values (higher k), this preload would be too small to influence stability. Although these same conditions exist for some points at tight clearances for the grooved journals also, there was no upswing effect noted in figure 18(b). The axial grooves could have had some effect on the tight clearance volumes to cancel any advantage in stability gained by preload due to slight misalinement of the bearing and journal.

In the tests in which the journals had tilted lobes, it was observed that the shaft speed could be increased beyond the point of initial fractional frequency whirl without the whirl orbit growing excessively. In some cases a shaft speed that was twice the shaft speed where initial fractional frequency whirl was reached before any sign of bearing distress (orbit growth or unsteady torque) was observed. This may be one of the best features of the tilted lobe-journal configuration.

Stability Comparison of Five Fixed Geometry Bearings

Whirl onset speed is plotted against radial clearance in figure 19 for five different fixed geometry journal bearings. The data for these curves were obtained from optimum locus curves for each bearing similar to those shown in figure 13(b) for the Rayleigh-step bearing. Figure 19 shows that the five fixed geometry bearings considered can be generally rated in order of diminishing stability as follows: (1) three-tilted-lobe bearing (offset factor of 1.0), (2) herringbone-groove bearing, (3) one-segment, three-pad, shrouded Rayleigh-step bearing, (4) three-tilted-lobe journal with grooves (offset factor of 1.0) mated with a plain bearing, and (5) three-centrally-lobed bearing with axial grooves (offset factor of 0.5). It is interesting to note that the commonly used centrally-lobed bearing has relatively poor stability when compared with the other four fixed geometry bearings. The herringbone-groove bearing stability curve crosses over the curves for the Rayleigh-step and the three-tilted-lobe journal with grooves at clearances of 0.034 and 0.037 millimeter (1340 and 1460 μin.), respectively. This type of cross-over pattern in the stability curves of various bearing types makes it difficult to rate one above the other. The ratings almost certainly require a qualifying range of clearance to make them worthwhile.

SUMMARY OF RESULTS

Stability tests were performed on a group of fixed geometry bearings which can be generally described as follows: (1) herringbone-groove bearings, (2) Rayleigh-step bearings, (3) three-lobed bearings, and (4) three-lobed journals mated with plain bearings. Various parameters

were altered to study their effect on stability of each class of bearing. The test bearings had a nominal 3.8 centimeters (1.5 in.) diameter and were 3.8 centimeters (1.5 in.) long. They were submerged in water at an average temperature of 300 K (80° F) and were operated hydrodynamically with zero load. The following results were obtained:

Herringbone-Groove Bearings

1. Groove length and number of grooves had no marked effect on stability when the data for journal bearings of approximately the same groove depths with 40, 20, and 10 partial and full grooves are taken as a whole.

2. The stability of the journal bearings with 40, 20, and 10 partial and full grooves was maximum when the groove to ridge clearance ratio was closest to 2.1 for a range of clearance values. This is as predicted by incompressible flow theory.

3. Maximum stability is achieved at the same groove to ridge clearance ratio as is the maximum radial force at a compressibility number of zero for a compressible lubricant, namely, at 2.1.

Rayleigh-Step-Bearings

1. The Rayleigh-step bearing configurations tested ranked in the following order of diminishing stability for clearances above 0.015 millimeter (600 μin.): one-segment, three-pad shrouded; one-segment, one-pad shrouded; one-segment, three-pad unshrouded; and three-segment, one-pad shrouded.

2. The stability of a three-segment, one-pad shrouded and a one-segment, three-pad shrouded bearing was not appreciably affected by a change in ridge to pad arc ratio from 0.40 to 0.49 and 0.27 to 0.45, respectively.

3. A substantial increase in stability can be gained with a shrouded compared to an unshrouded Rayleigh-step bearing.

4. For a one-segment, three-pad shrouded bearing there is an optimum value of film thickness ratio at any given clearance and this optimum is a function of clearance. Stability becomes more sensitive to film thickness ratio as clearance increases.

5. The optimum film thickness ratio for a stepped journal bearing is higher when stability rather than load capacity is used as the criterion.

Three-Lobe Bearings

1. Maximum stability of a three-lobe centrally-lobed bearing with axial grooves occurred at a lobe height of 0.025 millimeter (1000 μin.) over a clearance range of 0.015 to 0.052 millimeter (600 to 2050 μin.).

2. Stable operation of a three-lobe centrally-lobed bearing without axial grooves was impossible to attain at clearances above 0.018 millimeter (700 μin.) over a range of lobe heights from 0.025 to 0.102 millimeter (1000 to 4000 μin.).

3. Experiments indicate a smaller range of stable operation for three-lobe centrally-lobed bearings than predicted by theory.

4. An optimum value of preload coefficient exists at any given clearance, and this optimum is a function of clearance.

5. Experimental data indicate that, as the offset factor (angle from leading edge to the minimum-film-thickness point at zero eccentricity/lobe angle) of a three-lobe bearing is increased from 0.5 to 1.0, the stability increases and becomes less sensitive to clearance. This agrees well with theory, which predicts maximum stability at an offset factor of 0.9.

Three-Lobe Journals Mated with Plain Bearings

1. A plain bearing run with a tilted-lobe journal was more stable than a centrally-lobed journal at similar leading edge entrance wedge thickness values.

2. The incorporation of axial grooves in a tilted-lobe journal generally enhances its stability.

3. There is an optimum value of film thickness ratio at any given clearance for both the ungrooved and grooved journal, and this optimum is a function of clearance. Stability becomes more sensitive to film thickness ratio, for both types of journals, as clearance increases.

4. The range of optimum film thickness ratio is much greater for an ungrooved tilted-lobe journal (4.0 to 6.7), than for a grooved journal (1.55 to 1.92) which could make the ungrooved configuration more desirable for design purposes, even though it is generally less stable than the grooved journal.

5. In tests in which the journals had tilted lobes, it was observed that the shaft speed could be increased beyond the point of initial fractional frequency whirl without the whirl orbit growing excessively. In some cases a shaft speed that was twice the shaft speed where initial whirl occurred was reached before any sign of bearing distress (orbit growth or unsteady torque) was observed.

From this study five fixed geometry bearings considered can be generally rated in order of diminishing stability as follows: (1) three-tilted-lobe bearing (offset factor of 1.0), (2) herringbone-groove bearing, (3) one-segment, three-pad, shrouded Rayleigh-step bearing, (4) three-tilted-lobe journal with grooves (offset factor of 1.0) mated with a plain bearing, and (5) three-centrally-lobed bearing with grooves (offset factor of 0.5).

REFERENCES

1. Schuller, F. T., Anderson, W. J., and Nemeth, Z., "Experiments with Hydrodynamic Journal Bearings of Various Materials and Designs in Sodium at Temperatures to 800° F," Transactions of the ASLE, Vol. 11, No. 2, Apr. 1968, pp. 140-154.

2. Sternlicht, B., and Winn, L. W., "Geometry Effects on the Threshold of Half-Frequency Whirl in Self-Acting, Gas-Lubricated Journal Bearings," Journal of Basic Engineering, Vol. 86, No. 2, June 1964, pp. 313-320.

3. Malanoski, S. B., "Experiments on an Ultrastable Gas Journal Bearing," Journal of Lubrication Technology, Vol. 89, No. 4, Oct. 1967, pp. 433-438.

4. Vohr, J. H., and Chow, C. Y., "Characteristics of Herringbone-Grooved, Gas-Lubricated Journal Bearings," Journal of Basic Engineering, Vol. 87, No. 3, Sept. 1965, pp. 568-578.

5. Lund, J. W., "Rotor-Bearing Dynamics Design Technology. Part 7: The Three-Lobe Bearing and Floating Ring Bearing," MTI-67TR47, AFAPL-TR-65-45, pt. 7, AD-829895, Feb. 1968, Mechanical Technology, Inc., Latham, N.Y.

6. Marsh, H., "The Stability of Aerodynamic Gas Bearings. Part II: Noncircular Bearings," Ph.D. Dissertation 4525, June 1964, St. John's College, Cambridge.

7. Chadbourne, L. E., Dobler, F. X., and Rottler, A. D., "SNAP 50/SPUR Nuclear Mechanical Power Unit, Experimental Research and Development Program. Part 2: Bearings," APS-5249-R, AFAPL-TR-67-34, pt. 2, AD-815583, Dec. 1966, Garrett Corp., Phoenix, Ariz.

8. Schuller, F. T., Fleming, D. P., and Anderson, W. J., "Experiments on the Stability of Water Lubricated Herringbone-Groove Journal Bearings. I - Theoretical Considerations and Clearance Effects," TN D-4883, 1968, NASA, Cleveland, Ohio.

9. Schuller, F T., Fleming, D. P., and Anderson, W. J., "Experiments on the Stability of Water Lubricated Herringbone-Groove Journal Bearings. II - Effects of Configuration and Groove to Ridge Clearance Ratio," TN D-5264, 1969, NASA, Cleveland, Ohio.

10. Schuller, F. T., "Experiments on the Stability of Water-Lubricated Rayleigh Step Hydrodynamic Journal Bearings at Zero Load," TN D-6514, 1971, NASA, Cleveland, Ohio.

11. Schuller, F. T., "Experiments on the Stability of Water-Lubricated Three-Lobe Hydrodynamic Journal Bearings at Zero Load," TN D-6315, 1971, NASA, Cleveland, Ohio.

12. Schuller, F. T., and Anderson, W. J., "Experiments on the Stability of Water-Lubricated Three-Sector Hydrodynamic Journal Bearings at Zero Load," TN D-5752, 1970, NASA, Cleveland, Ohio.

13. Schuller, F. T., "Experiments on the Stability of Water-Lubricated Three-Lobe Journals Mated with Plain Bearings at Zero Load," Proposed NASA Technical Note.

14. Hamrock, B. J., and Anderson, W. J., "Incompressibly Lubricated Raleigh Step Journal Bearing. II - Infinite-Length Solution," TN D-4873, 1968, NASA, Cleveland, Ohio.

15. Hamrock, B. J., and Anderson, W. J., "Rayleigh Step Journal Bearing. Part II - Incompressible Fluid," Journal of Lubrication Technology, Vol. 91, No. 4, Oct. 1969, pp. 641-650.

16. Lund, J. W., ed., "Design Handbook for Fluid Film Type Bearings. Part III of Rotor-Bearing Dynamics Design Technology." MTI-65TR14, AFAPL TR-65-Pt. III, Ad-466392, May 1965, Mechanical Technology, Inc., Latham, N.Y.

17. Falkenhagen, G. L., Gunter, E. J., and Schuller, F. T., "Stability and Transient Motion of a Vertical Three-Lobe Bearing System," Paper 71-Vibr-76, Sept. 1971, ASME, New York, N.Y.

18. Boeker, G. G., and Sternlicht, B., "Investigation of Translatory Fluid Whirl in Vertical Machines," Transactions of the ASME, Vol. 78, No. 1, Jan. 1956, pp. 13-19.

E-6710

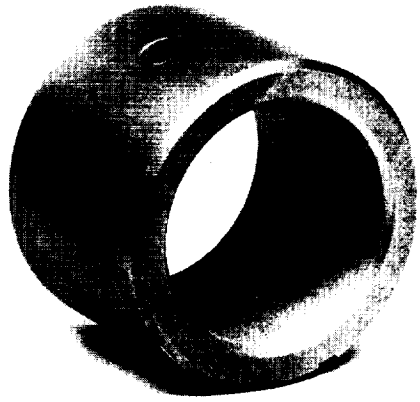

C-68-2882

Plain bearing

10 partial grooves

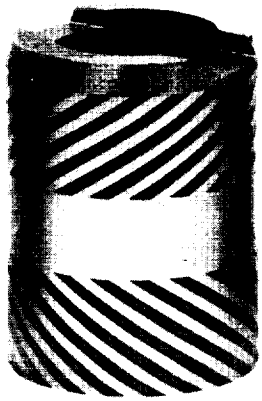

20 partial grooves

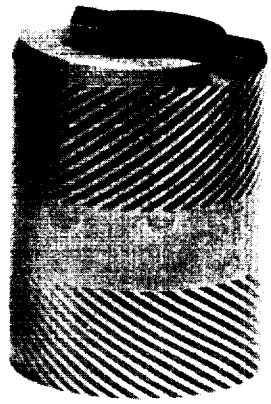

40 partial grooves

C-68-2881

10 full grooves

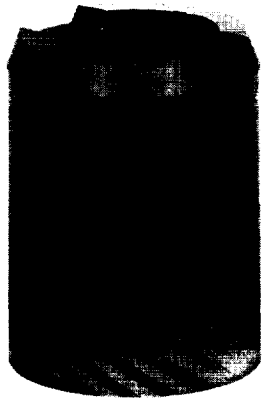

20 full grooves

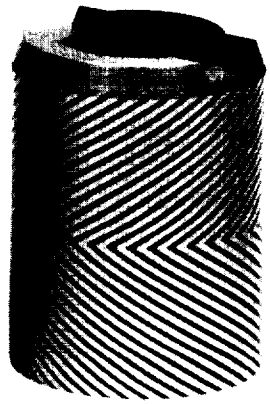

40 full grooves

C-68-2880

(a) Configurations.

Figure 1. - Herringbone-grooved journal.

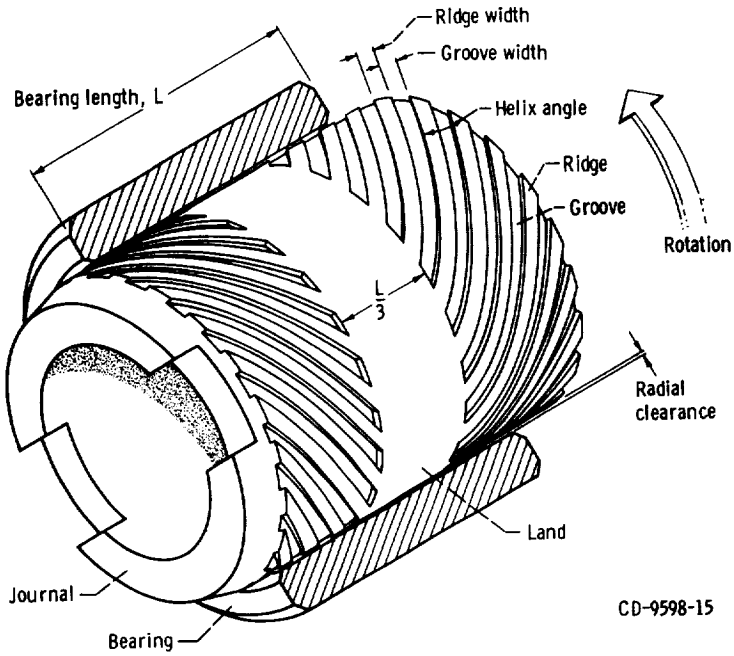

(b) Bearing assembly.

Figure 1. - Concluded.

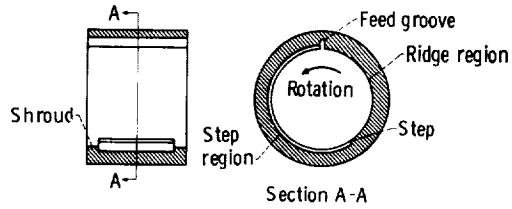

(a) One-segment, one-pad shrouded Rayleigh-step journal bearing.

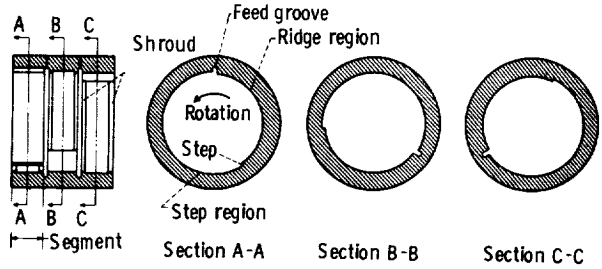

(b) Three-segment, one-pad shrouded Rayleigh-step journal bearing.

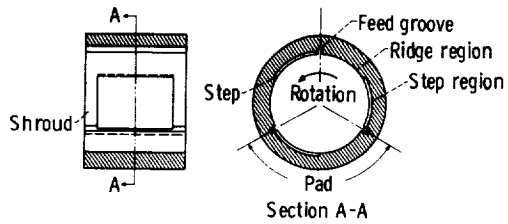

(c) One-segment, three-pad shrouded Rayleigh-step journal bearing.

Figure 2. - Rayleigh-step bearing configurations.

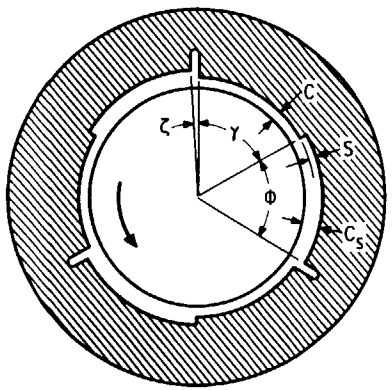

Figure 3. - Rayleigh–step bearing geometry. Ridge to pad arc ratio $\psi = \gamma/(\gamma + \Phi + \zeta)$; film thickness ratio $k_r = C_S/C$.

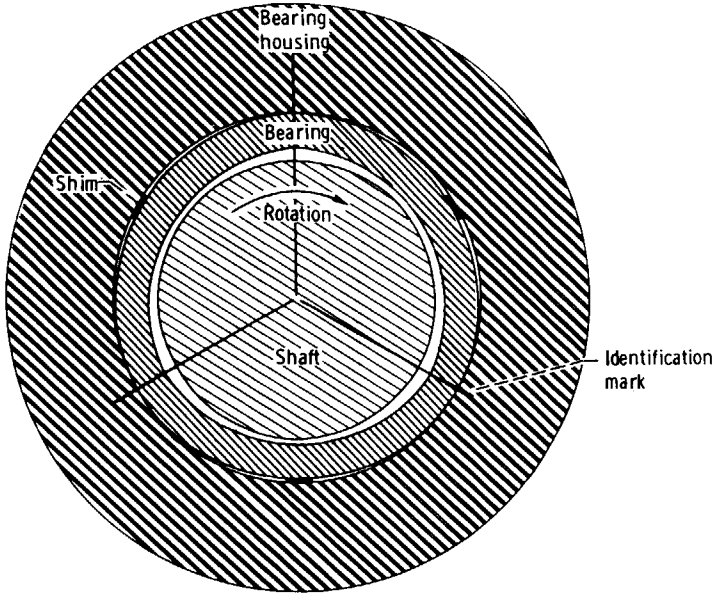

(a) Bearing assembly.

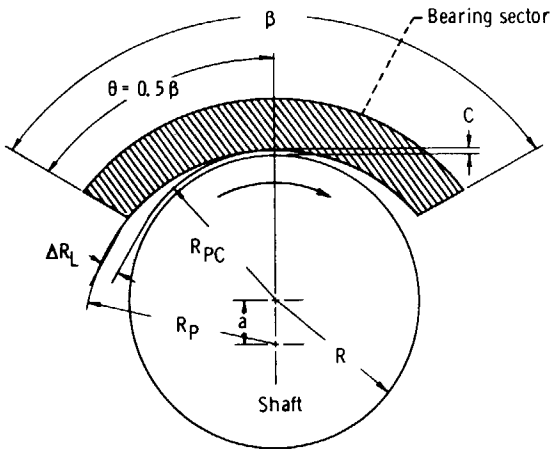

(b) Bearing geometry. Offset factor, $\alpha = \theta/\beta = 0.5$.

Figure 4. - Three-centrally-lobed bearing.

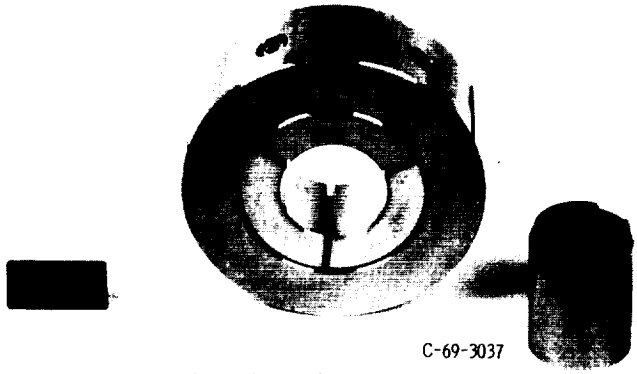

(a) Assembled bearing configuration.

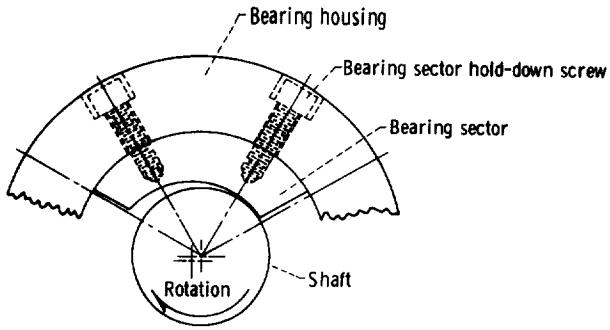

(b) Bearing sector assembly.

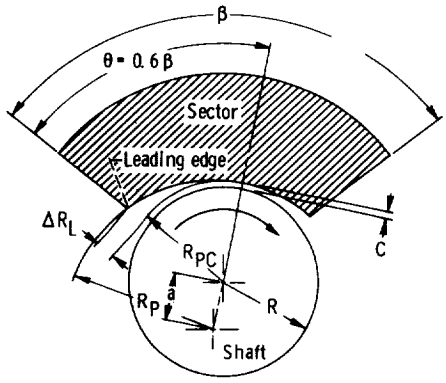

(c) Converging-diverging configuration. Offset factor, $\alpha = \theta/\beta = 0.6$.

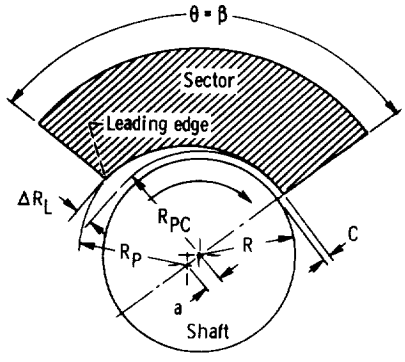

(d) Wholly-converging configuration. Offset factor, $\alpha = \theta/\beta = 1.0$.

Figure 5. - Three-sector bearing.

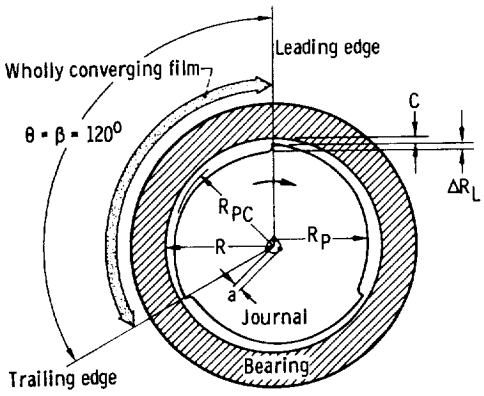

(a) Tilted-lobe (wholly-converging) configuration offset factor, $\alpha = \theta/\beta = 1.0$.

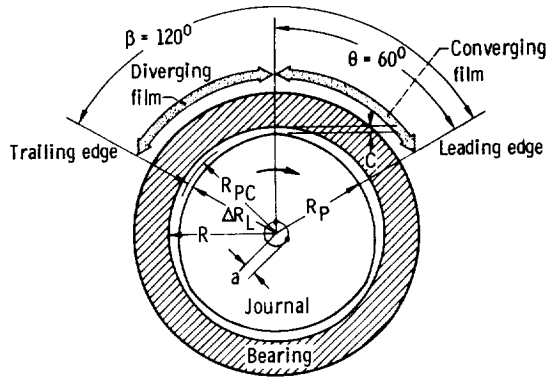

(b) Centrally-lobed (converging-diverging) configuration offset factor, $\alpha = \theta/\beta = 0.5$.

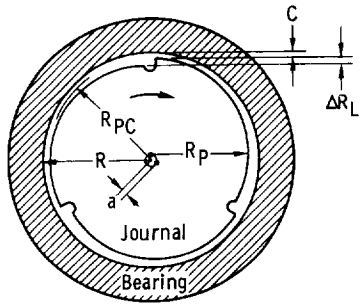

(c) Tilted-lobe (wholly-converging) configuration with three axial grooves.

Figure 6. - Three-lobe journal geometry.

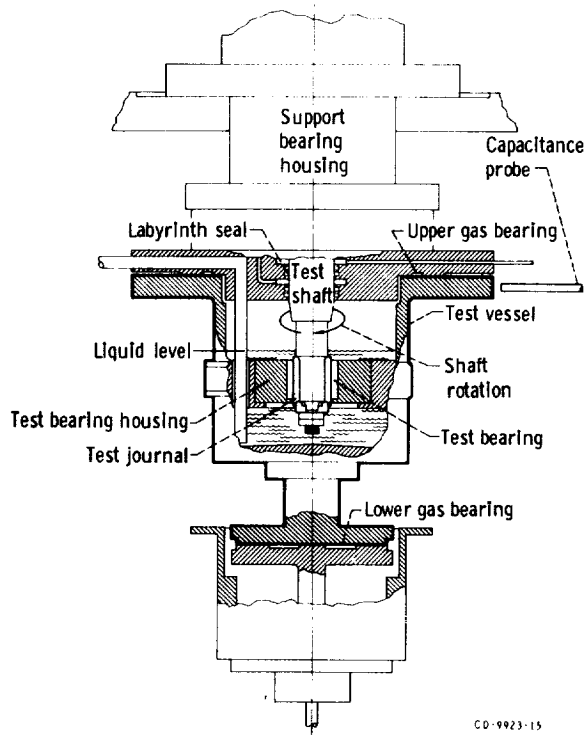

Figure 7. - Bearing test apparatus.

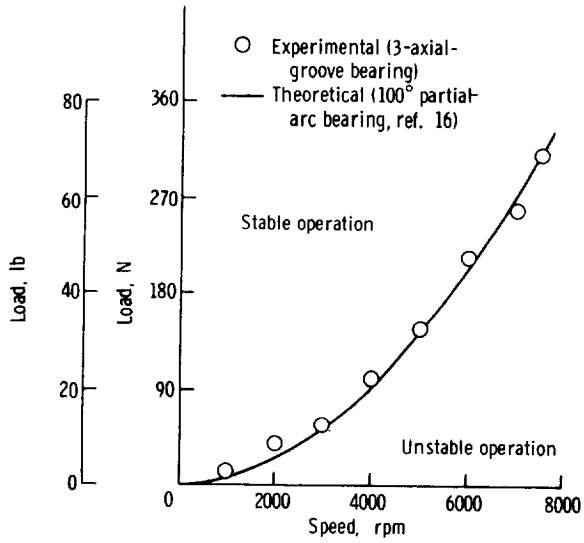

Figure 8. - Comparison of theoretical stability characteristics of 100° partial-arc bearing with experimental data for three-axial-groove bearing. Length to diameter ratio, 1; radial clearance, 20 microns (0.0008 in.).

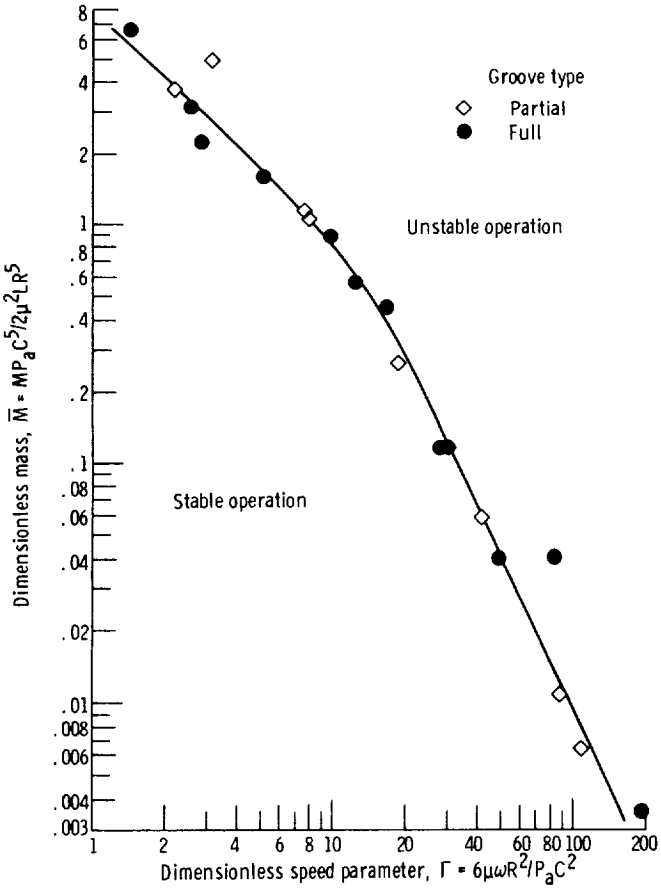

Figure 9. - Mean stability of herringbone journal bearings with 10, 20, and 40 partial and full grooves. Range of groove depth, 0.032 to 0.043 millimeter (1280 to 1700 μin.).

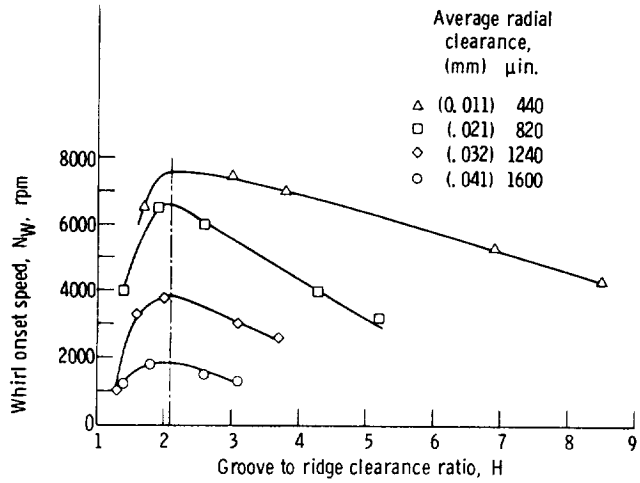

Figure 10. - Effect of groove to ridge clearance ratio on stability of herringbone journal bearing with 10 partial grooves in water (zero load).

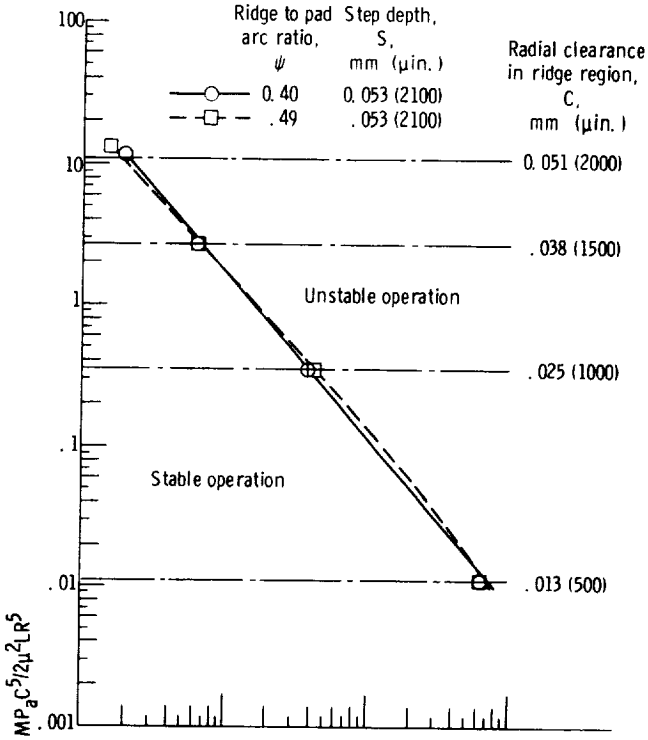

(a) Three-segment, one-pad shrouded Rayleigh-step bearing.

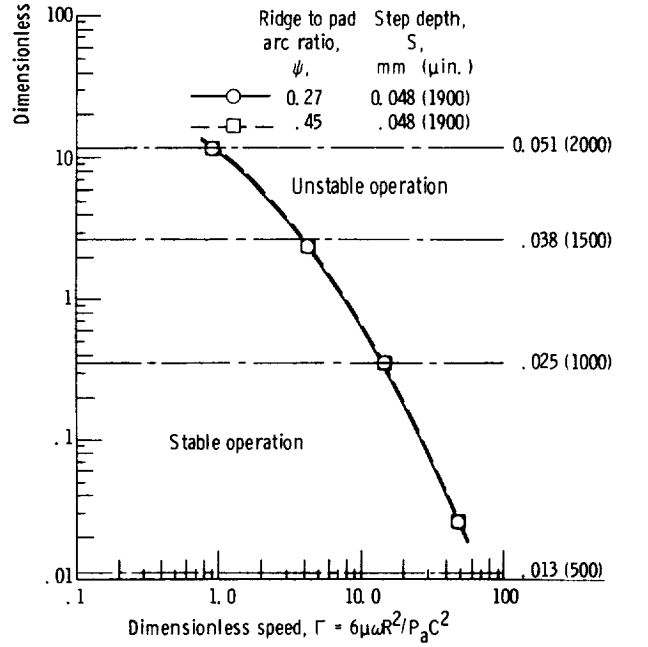

(b) One-segment, three-pad shrouded Rayleigh-step bearing.

Figure 11. - Effect of ridge to pad arc ratio ψ on stability.

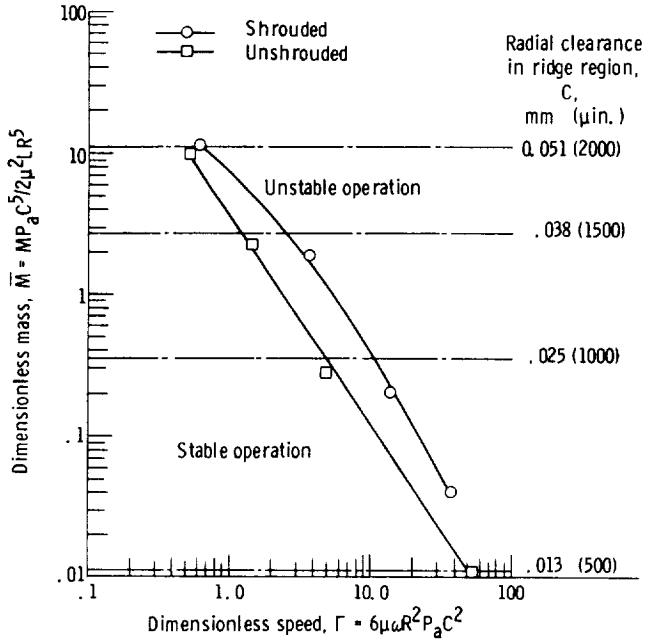

Figure 12. - Comparison of stability of shrouded and unshrouded one-segment, three-pad Rayleigh-step bearing. Ridge to pad arc ratio $\psi = 0.45$; step depth S = 0.066 millimeter (2600 μin.).

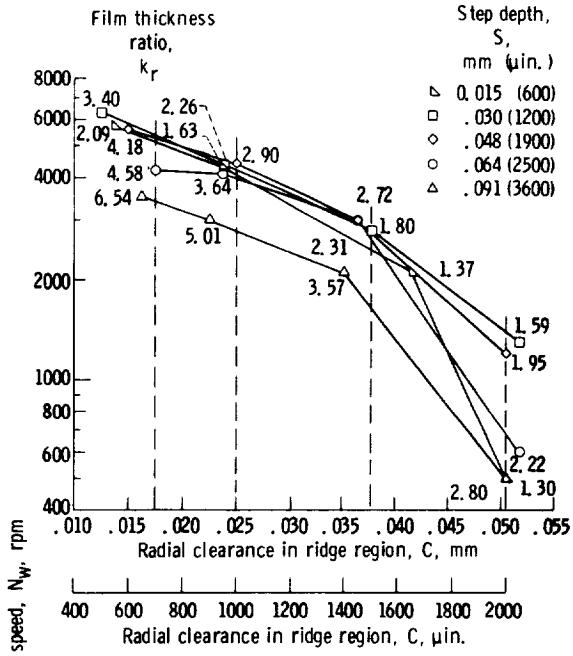

(a) Whirl onset speed as a function of radial clearance.

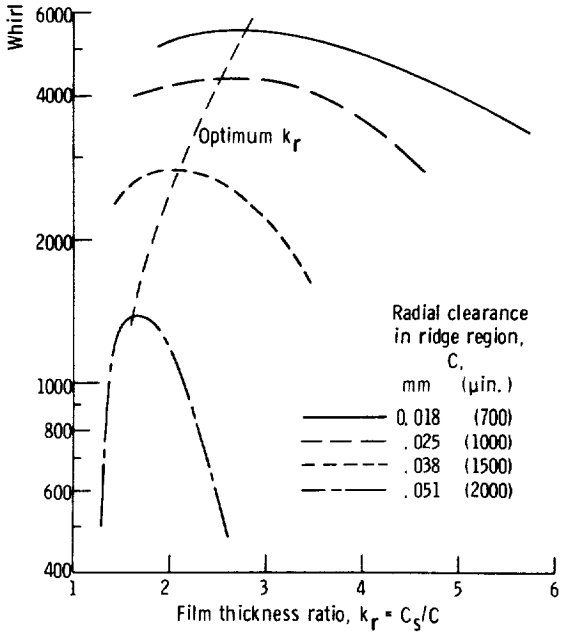

(b) Whirl onset speed as a function of film thickness ratio.

Figure 13. - Effect of radial clearance and film thickness ratio on the stability of a one-segment, three-pad shrouded Rayleigh-step bearing. Ridge to pad arc ratio $\psi = 0.27$.

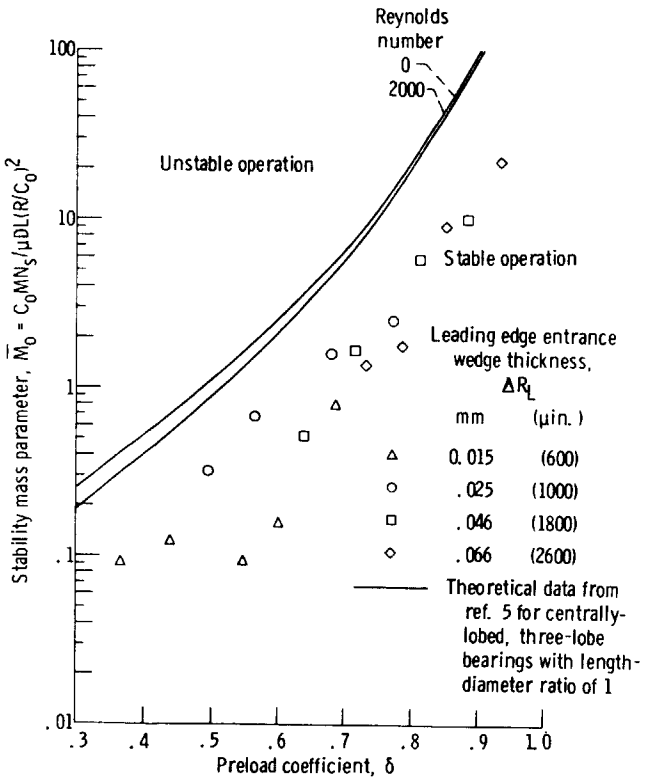

Figure 14. - Comparison of theoretical and experimental data for three-centrally-lobed bearings with axial grooves using dimensionless parameters of reference 5.

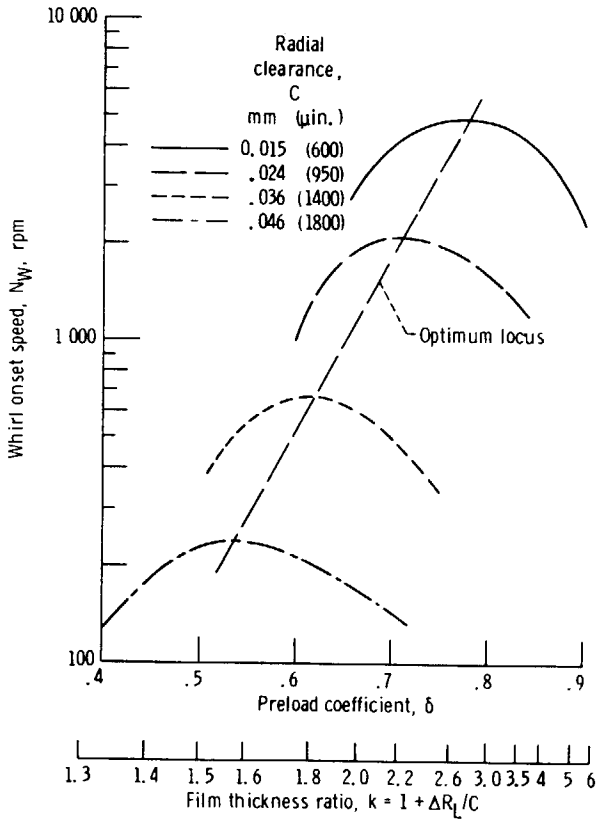

Figure 15. - Whirl onset speed as function of preload coefficient and film thickness ratio for three-lobe-centrally lobed bearing with axial grooves.

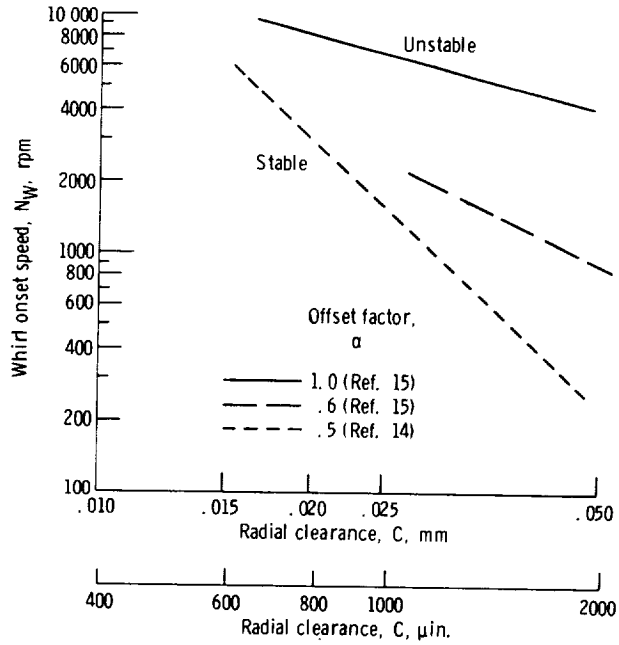

Figure 16. - Comparison of stability of three-lobe bearings at various offset factors.

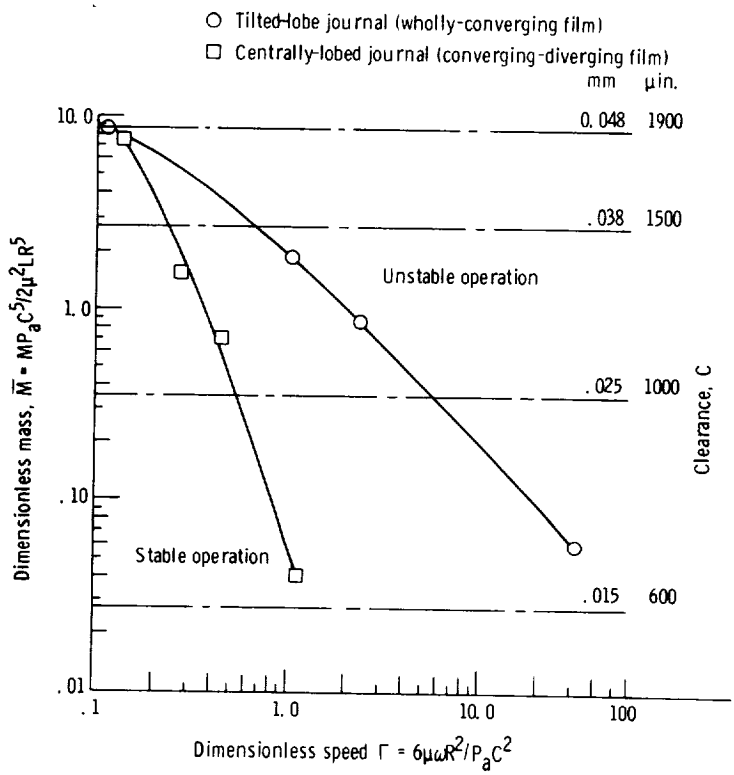

Figure 17. - Comparison of the stability of a wholly-converging and a converging-diverging film configuration. Journal leading edge entrance wedge thickness, 0.023 mm (900 μin.). No grooves in journals.

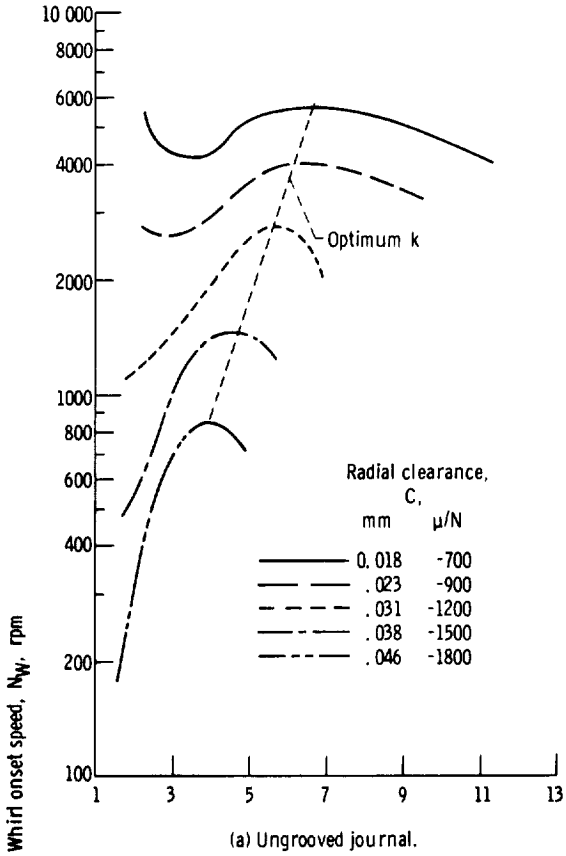

(a) Ungrooved journal.

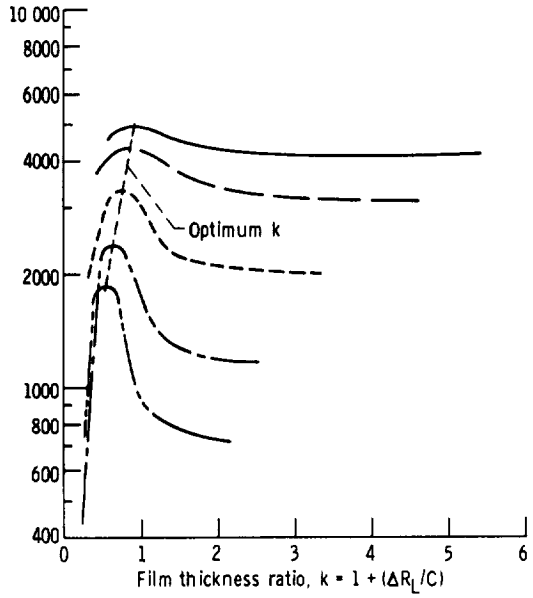

(b) Grooved journal.

Figure 18. - Whirl onset speed as function of film thickness ratio.

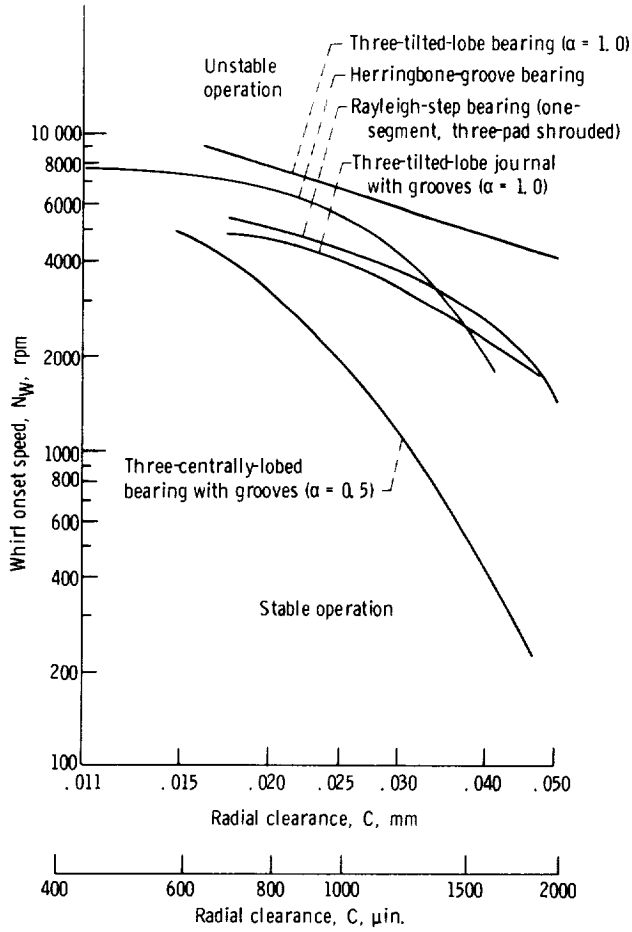

Figure 19. - Stability of five fixed geometry bearings.